ACS APPLIED MATERIALS & INTERFACES

Research Article

www.acsami.org

A Chemometric Approach for the Sensitization Procedure of ZnO Flowerlike Microstructures for Dye-Sensitized Solar Cells

Diego Pugliese,*[,†,‡] Federico Bella,[†,‡] Valentina Cauda,[‡] Andrea Lamberti,[†,‡] Adriano Sacco,[‡] Elena Tresso,[†,‡] and Stefano Bianco[‡]

[†]Department of Applied Science and Technology, Politecnico di Torino, C.so Duca degli Abruzzi 24, 10129 Torino, Italy

[‡]Center for Space Human Robotics @PoliTo, Istituto Italiano di Tecnologia, C.so Trento 21, 10129 Torino, Italy

Supporting Information

ABSTRACT: In this paper, a methodology for the streamlining of the sensitization procedure of flowerlike ZnO nanostructures for dye-sensitized solar cells (DSCs) is reported. The sensitization of ZnO surface with ruthenium-based complexes is a particularly critical process, since one has to minimize the dissolution of surface Zn atoms by the protons released from the dye molecules, leading to the formation of Zn^{2+}/dye complexes. The fine-tuning of the experimental parameters, such as the dye loading time, the dye concentration, and the pH of the sensitizing solution, performed through a multivariate optimization by means of a chemometric approach, is here reported. The dye loading procedure was optimized using ZnO microparticles with nanostructured protrusions, synthesized by a simple and low-cost hydrothermal process. Mild reaction conditions were used, and wurtzite-like crystalline structure with a relatively high surface area was obtained once the reaction process was completed. After dispersion of ZnO flowerlike particles in an acetic acid-based solution, a 14 μm-thick ZnO layer acting as DSC photoanode was fabricated. The optimized sensitization procedure allowed minimizing the instability of ZnO surface in contact with acidic dyes, avoiding the formation of molecular agglomerates unable to inject electrons in the ZnO conduction band, achieving good results in the photoconversion efficiency. Moreover, the photoharvesting properties were further enhanced by adding *N*-methylbenzimidazole into the iodine-based liquid electrolyte. Such an additive was proposed here for the first time in combination with a ZnO photoelectrode, helping to reduce an undesired recombination between the photoinjected electrons and the oxidized redox mediator.

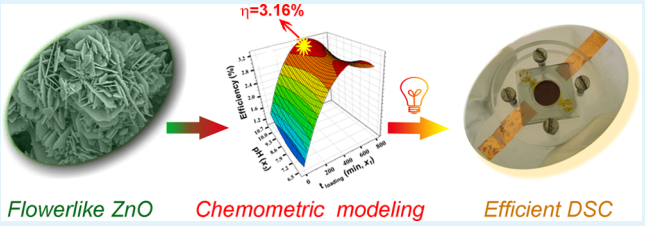

KEYWORDS: *dye-sensitized solar cell, zinc oxide, flowerlike nanostructure, microfluidic cell, N-methylbenzimidazole, design of experiments*

1. INTRODUCTION

As one of the major renewable energy sources, solar energy has the potential to become an essential component in the future of global energy production. Since the breakthrough work reported by O'Regan and Grätzel in 1991,[1] intensive interest was devoted to dye-sensitized solar cells (DSCs) due to their low cost, highly efficient conversion of visible light into electricity, and ecofriendly production. DSCs represent one of the most promising strategies among several alternatives to conventional silicon solar cells, due to the cost-effective concept for solar-to-electric energy conversion.[2,3] A typical DSC consists of a dye-coated TiO_2 nanocrystalline electrode, which is deposited on a fluorine-doped tin oxide (FTO) conductive-glass substrate, a I^-/I_3^--based electrolyte and a platinum counter electrode. Upon illumination, the dye molecules inject electrons into the conduction band of the semiconducting TiO_2. Electrons then diffuse through the TiO_2 nanocrystalline film and are collected at the FTO front-contact. A closed regenerative circuit is achieved by the redox couple ions present in the electrolyte, which drain electrons from the external circuit at the counter electrode and reduce the oxidized molecules of the dye.[4]

At present, the wide band gap semiconductor TiO_2 has been by far the most broadly used DSC photoelectrode material, with a maximum photovoltaic conversion efficiency that exceeds 12%[5] in liquid cells. Besides TiO_2, a series of other n-type metal oxide semiconductors were explored as potential anodes in DSCs, such as ZnO, SnO_2 and In_2O_3.[6] However, up to now, no other material has reached efficiencies comparable to those of titanium dioxide.

Zinc oxide, a direct wide band gap (3.37 eV) semiconductor with a large exciton binding energy (60 MeV), is considered to be one of the most promising semiconductor materials for applications in optoelectronics, sensors and field emission devices.[7−9] The wurtzite structure is a hexagonal close packing crystal system, with no center of inversion and therefore an

Received: August 21, 2013
Accepted: October 8, 2013
Published: October 8, 2013

inherent asymmetry along the major *c*-axis. This feature allows the anisotropic growth of the crystal along the [001] direction and, based on a wide range of synthesis routes,[10,11] a very rich variety of ZnO nanostructures can be obtained. Their morphologies include highly ordered nanowire and nanorod arrays,[12] nanotubes,[13] nanobelts,[14] nanosheets,[15] nanoplants,[16] and nanotetrapods.[17] These quasi-one-dimensional (1-D) structures have attracted a great research interest for applications in field effect transistors,[18] optoelectronics,[19] field emission devices,[20] and piezoelectricity.[21,22] Recently, great interest was also paid to ZnO in the field of DSCs[23] owing to its higher electron mobility and similar electronic band structure with respect to those of TiO_2.[24] For all these reasons, ZnO is now considered as the second most used semiconductor for solar energy conversion by means of third generation devices.[25] However, despite the many efforts spent to improve the performance of ZnO-based dye-sensitized solar cells, the light-to-electricity conversion efficiency remains lower than the one of TiO_2-based cells. Actually, the most efficient ZnO-based DSC was achieved by Memarian et al.,[26] who obtained a 7.5% overall efficiency, around half of the maximum performance obtained for TiO_2.[5]

The main reason which prevents zinc oxide from achieving photoconversion performances comparable to those obtained for TiO_2 is the remarkably critical sensitization procedure of this semiconductor with Ru-based dyes. In particular, the presence of carboxylic acid binding groups of Ru dyes can lead to the dissolution of ZnO and the precipitation of molecular Zn^{2+}/dye complexes, resulting in reduced overall electron injection efficiency by the excited dye.[27] Several approaches were performed to overcome these sensitization problems. Keis et al.[28] obtained 5% of efficiency by adding KOH to the acidic dye-loading solutions and shortening the loading time. Other researchers[29,30] claimed that an improvement of dye loading can be achieved by changing the microstructure of the ZnO films, thus avoiding complex formation without the need of basic dye solutions.[31] However, these works were focused on the investigation of specific aspects of the preparation and sensitization procedure of ZnO: a multivariate and comprehensive study of the critical points listed above has never been performed. For all these reasons, the aim of the present work is to define an optimal sensitization procedure for flowerlike ZnO nanostructured microparticles for the fabrication of efficient DSC photoanodes. In order to overcome the important drawback of the formation of N719 dye/ZnO aggregates and to achieve high conversion efficiency, a multivariate optimization of the experimental conditions was carried out. In particular, dye loading time, dye concentration, and pH of the sensitizing solution were investigated by means of a chemometric approach,[32] which was adopted here for the first time in ZnO-based DSC fabrication. The fabricated solar cells were studied by current−voltage (*I*−*V*) electrical characterization, incident photon-to-electron conversion efficiency (IPCE), and electrochemical impedance spectroscopy (EIS) measurements. Furthermore, the effect of *N*-methylbenzimidazole as a liquid electrolyte additive in a ZnO-based DSC was not previously reported.

Although the findings we report here are related with the sensitization of a ZnO nanostructure with a ruthenium-based dye, the concepts we deepened are dramatically more general. The chemometric approach is a very powerful technique for the fine-tuning of the experimental parameters in the development of a device, its applicability is widespread, and it is particularly suitable for the refinement of the performances of devices avoiding the "trial and error" approach which is usually suited. This work would like to pave the way to an experimental procedure that can find application in many other different aspects of the optimization of DSCs.

2. EXPERIMENTAL SECTION

2.1. ZnO Flowerlike Microstructures: Synthesis and Characterization. Amounts of 0.56 g of potassium hydroxide (KOH, 1 M, purchased from Merck) and 1.48 g of zinc nitrate hexahydrate ($ZnNO_3{\cdot}6H_2O$, 0.5 M, purchased from Sigma-Aldrich) were both dissolved separately in 10 mL of bidistilled water (from Direct-Q system, Millipore).[33] Then, the zinc nitrate solution was dropped into KOH under vigorous stirring, obtaining a white gel. The gel was placed in a closed Teflon bottle at 70 °C. After 4 h, ZnO particles were carefully separated from the solution by filtration, washed repetitively with deionized water until the pH neutralization, and dried at 60 °C overnight in air.

The morphology of the ZnO microparticles was investigated by means of field emission scanning electron microscopy (FESEM, Dual Beam Auriga from Carl Zeiss, operating at 5 keV). Brunauer−Emmett−Teller (BET) specific surface area was measured from N_2 sorption isotherms (Quadrasorb SI, Quantachrome) by multipoint method within the relative pressure range of 0.1−0.3 P/P_0. Density functional theory (DFT) model was applied to estimate the pore size distribution of the flowerlike ZnO particles. X-ray diffraction technique was used to determine the crystalline structure of the powder (X'Pert diffractogram, Cu Kα = 1.54 Å).

2.2. DSC Fabrication and Characterization. ZnO flowerlike particles were dispersed in a solution containing acetic acid (1 vol %), ethanol (67 vol %), and water (33 vol %) in a weight ratio of 1:2 (ZnO/solution)[29] and then sonicated for 4 h in order to obtain a homogeneous paste. Subsequently, a circular shaped ZnO layer was deposited using the tape-casting technique on FTO covered glasses (7 Ω/sq, Solaronix) preliminarily cleaned using a procedure described elsewhere.[34] The coated films were initially dried at 90 °C for 30 min and then thermally treated at 450 °C for 10 min in air. The final thickness of ZnO film was about 14 μm, as measured by using a profilometer (P.10 KLA-Tencor Profiler). Photoelectrodes were then heated at 70 °C and soaked in a N719 ethanol-based sensitizing solution (Ruthenizer 535bis-TBA, Solaronix) at room temperature and finally rinsed in pure ethanol to remove the weakly or nonadsorbed dye molecules. Different dye immersion times and different values for the pH and the dye concentration of the sensitizing solution were investigated. Counter electrode fabrication and cell assembly procedures were reported in previous works.[31,34] A commercial liquid electrolyte solution (Iodolyte AN 50, Solaronix) was employed and, where specified, *N*-methylbenzimidazole was added in the electrolyte solution.

I−*V* electrical characterization was carried out using a source measure unit (model 2440, Keithley) and a solar simulator (model 91195A, Newport) under AM1.5G irradiation, with power output (100 mW/cm^2) calibrated by a Si reference solar cell. IPCE measurements were performed in DC mode using a source measure unit (model 2440, Keithley), illuminating the cells through a monochromatic beam provided by a 100 W QTH lamp (Newport) and a monochromator (model Omni-λ 150, Lot-Oriel), without bias light. Electrochemical impedance spectra were collected in dark conditions using an electrochemical workstation (760D, CH Instruments) in the frequency range 100 mHz to 100 kHz at different applied bias voltages, with an AC signal amplitude of 10 mV.

2.3. Chemometric Approach. Chemometrics is the mathematical approach which converts experimental data into useful information for decision-making in science.[35] Nowadays, the strong imbalance that exists between the technical ability to generate a large amount of excellent experimental data and the human ability to properly interpret it is quite worrying. To overcome this, chemometric methods (in particular the design of experiments, DoE) were proposed: the main goal is to plan the type and the number of experiments required to

obtain the maximum possible information from the investigated system, reducing concurrently the overall number of experiments.

The first step entails the selection of the variables to be investigated and their relative experimental domain. In agreement with the purpose of the work, the chosen experimental variables were the dye loading time (x_1), the dye solution concentration (x_2) and its pH (x_3). The selected ranks of the values associated with the variables were the following: x_1 was between 2 and 780 min, x_2 ranged between 0.05 and 0.75 mM, and x_3 from 6.5 to 10.7. In order to carry out a multivariate DoE, the software MODDE (version 7.0.0.1, Umetrics), widely used in chemistry[36] and materials science,[37] was adopted. An experimental domain as the one considered here can be investigated by means of a factorial design, which has cubical geometry and is able to study the influence of all factors (experimental variables) on the selected response (efficiency of sunlight conversion). A particular factorial design is the central composite face-centered (CCF): in this case, the experiments are carried out not only on the vertices, but axial points on the faces of the factorial hypercube are added (see Figure S-1 in the Supporting Information). Each factor is studied on 3 levels (−1, 0, +1), with a total of 17 experiments, as detailed in subsection 3.2. A thorough discussion of the statistical and mathematical basis behind the chosen DoE can also be found elsewhere.[38]

3. RESULTS AND DISCUSSION

3.1. ZnO Flowerlike Microstructure Characterization. X-ray Diffraction (XRD) patterns of ZnO flowerlike microparticles prepared at 70 °C are reported in Figure 1. The diffraction peaks show the good crystalline quality of the sample, with the presence of a pure hexagonal wurtzite structure (JCPDS file, No. 80-0074).

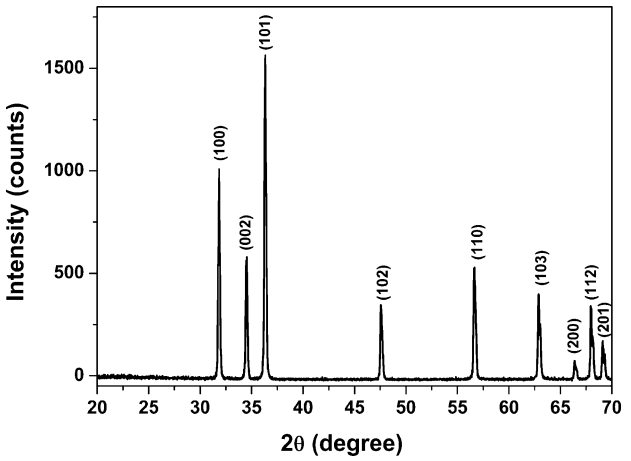

Figure 1. XRD patterns of ZnO flowerlike microparticles prepared at 70 °C.

Figure 2 shows FESEM images of ZnO flowerlike particles and of ZnO film after drying at 90 °C and subsequently heating at 450 °C. Zinc oxide powder is composed of nearly spherical particles with regular nanostructured prism-shaped planes as building blocks. The branched and nanostructured morphology of ZnO is still well maintained after the preparation of the photoanode, with only a slight smoothing of the sharp edges due to the little dissolution effect of acetic acid-based solution. However, the XRD pattern after the photoanode preparation did not show any degradation of the crystalline wurtzite structure (data not reported).

The specific surface area, as measured by BET approach, is 19.58 m^2/g, in line with the value measured for nanoporous ZnO electrodes.[28] Flowerlike ZnO particles also show some degree of nanoporosity, evaluated by DFT model, with pore size distribution peaking at about 4 nm. The N_2 sorption isotherm and DFT pore size distribution are reported in the Supporting Information (Figure S-2).

3.2. Chemometric Investigation of Photovoltaic Performances. The sensitization of the ZnO flowerlike microparticles and the resulting performances on lab-scale DSCs were investigated by means of a CCF-DoE, a multivariate analysis method which permits the optimization of functional materials, simultaneously determining variables as others are modified. With this mathematical technique, the operational variables (dye loading time x_1, dye solution concentration x_2, and its pH x_3) can be simultaneously changed in order to identify the weight of each one and the relationship between them, indicating antagonisms and synergies. To the best of our knowledge, most of the investigations about DSCs consist of a monovariate analysis, even if this procedure leads to error when, at the very least, interactions between the variables occur. For all these reasons, an experimental design that simultaneously studies different variables is necessary to obtain an empirical mathematical equation for all the factors involved, as well as a response map that considers the influence of all the parameters.

Table 1 presents the experimental matrix generated by the software for the adopted CCF-DoE. As experimental response (y), it was decided to evaluate the light-to-electricity conversion efficiency (η) under 1 sun. In order to assess the experimental reproducibility, three replicas (F15, F16, F17) of the central point were carried out. In fact, the DoE reproducibility is usually evaluated on the experimental point with all the variables at their intermediate value. However, since the study of the reproducibility on a single experiment might seem insufficient, a second step of validation of the chemometric model will be introduced later.

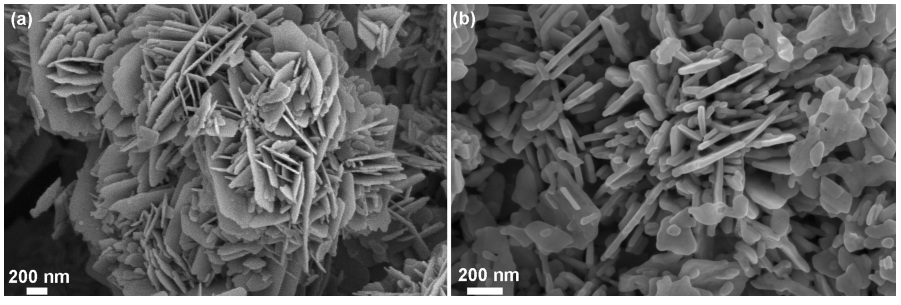

Figure 2. (a) FESEM image of ZnO flowerlike microparticles prepared at 70 °C and (b) FESEM image of ZnO film after drying at 90 °C and subsequently heating at 450 °C.

Table 1. Experimental Matrix of Variables and Corresponding Experimental and Predicted Responses to Optimize Sunlight Conversion Efficiency[a]

exp. name	dye loading time (x_1, min)	dye concentration (x_2, mM)	dye solution pH (x_3)	η observed (y, %)	η predicted (%)	J_{sc} (mA/cm^2)	V_{oc} (V)	FF
F1	2 (−1)	0.05 (−1)	6.5 (−1)	0.24	0.19	0.82	0.46	0.62
F2	780 (+1)	0.05 (−1)	6.5 (−1)	2.85	2.92	8.96	0.55	0.58
F3	2 (−1)	0.05 (−1)	10.7 (+1)	0.22	0.25	0.79	0.46	0.61
F4	780 (+1)	0.05 (−1)	10.7 (+1)	2.68	2.66	7.54	0.54	0.66
F5	2 (−1)	0.75 (+1)	6.5 (−1)	1.12	1.13	3.08	0.53	0.69
F6	780 (+1)	0.75 (+1)	6.5 (−1)	2.22	2.19	6.04	0.58	0.64
F7	2 (−1)	0.75 (+1)	10.7 (+1)	1.77	1.69	4.64	0.55	0.69
F8	780 (+1)	0.75 (+1)	10.7 (+1)	2.37	2.42	7.11	0.57	0.59
F9	2 (−1)	0.4 (0)	8.6 (0)	0.92	1.01	2.57	0.53	0.68
F10	780 (+1)	0.4 (0)	8.6 (0)	2.81	2.74	7.31	0.59	0.66
F11	391 (0)	0.4 (0)	6.5 (−1)	3.04	3.04	7.98	0.58	0.65
F12	391 (0)	0.4 (0)	10.7 (+1)	3.16	3.18	8.57	0.56	0.65
F13	391 (0)	0.05 (−1)	8.6 (0)	2.28	2.25	7.31	0.52	0.60
F14	391 (0)	0.75 (+1)	8.6 (0)	2.55	2.60	7.58	0.57	0.59
F15	391 (0)	0.4 (0)	8.6 (0)	2.73	2.86	8.22	0.58	0.57
F16	391 (0)	0.4 (0)	8.6 (0)	2.87	2.86	8.46	0.58	0.59
F17	391 (0)	0.4 (0)	8.6 (0)	3.03	2.86	8.33	0.57	0.64

[a]For completeness, short circuit current density (J_{sc}), open circuit voltage (V_{oc}), and fill factor (FF) values are also reported. Each variable was investigated at three levels (−1, 0, +1).

The set of carried out experiments allowed to achieve a maximum light-to-electricity conversion efficiency of 3.16% (short circuit current density J_{sc} = 8.57 mA/cm^2, open circuit voltage V_{oc} = 0.56 V, fill factor FF = 0.65) for the ZnO photoelectrode sensitized with a 0.40 mM dye solution (pH 10.7) for 391 min (6.5 h). The current density−voltage curve and the corresponding IPCE curve of the DSC with the highest photoconversion efficiency, as mentioned above, are reported in Figure 3. Multiple linear regression interpolation parameters

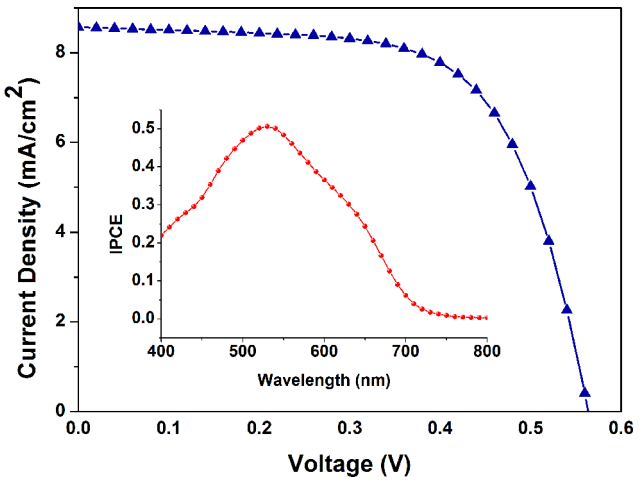

Figure 3. Current density−voltage curve of the DSC (experiment F12 in Table 1) with the highest photoconversion efficiency. The corresponding IPCE curve is shown in the inset.

were R^2 = 0.99 and Q^2 = 0.96. For the sake of completion, R^2 represents the fraction of the response variation explained by the model and Q^2 is the fraction of the response variation that can be predicted by the model. More broadly, R^2 and Q^2 provide the summary of the fit of the model: R^2 is an overestimated measure and Q^2 an underestimated value of the goodness of the fitting model. Both of these values are very close to 1, meaning that the regression model provides an excellent description of the relationship between the independent variables and the response, and therefore an optimal analysis of the investigated system. Additional plots and statistical parameters useful for evaluating the goodness of the chemometric model are shown in Figures S-3 and S-4 in the Supporting Information. Furthermore, the average value of sunlight conversion efficiency for the three replicated cells (from F15 to F17) was 2.88 (±0.13)%: this value is not only an excellent index of reproducibility, if compared to the repeatability typically observed in the literature for the DSC devices, but it also perfectly corresponds to the theoretical value predicted by the chemometric model (2.86%).

Figure 4 shows the influence (with 95% confidence) of each experimental factor on the response y (sunlight conversion

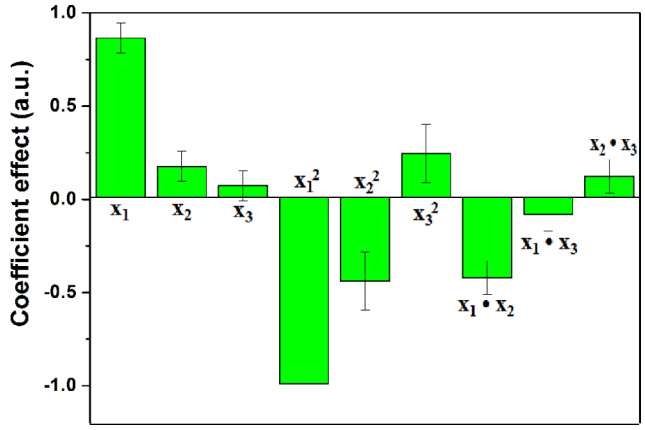

Figure 4. Coefficient plot for the CCF-DoE. x_1 is the dye loading time, x_2 is the dye solution concentration, and x_3 is the pH of dye solution.

efficiency). This coefficient plot is useful to develop the final modeling equation, which is an empirical relationship between the response and the factors expressed in polynomial form. From the ANOVA statistical analysis, it results in the following equation:

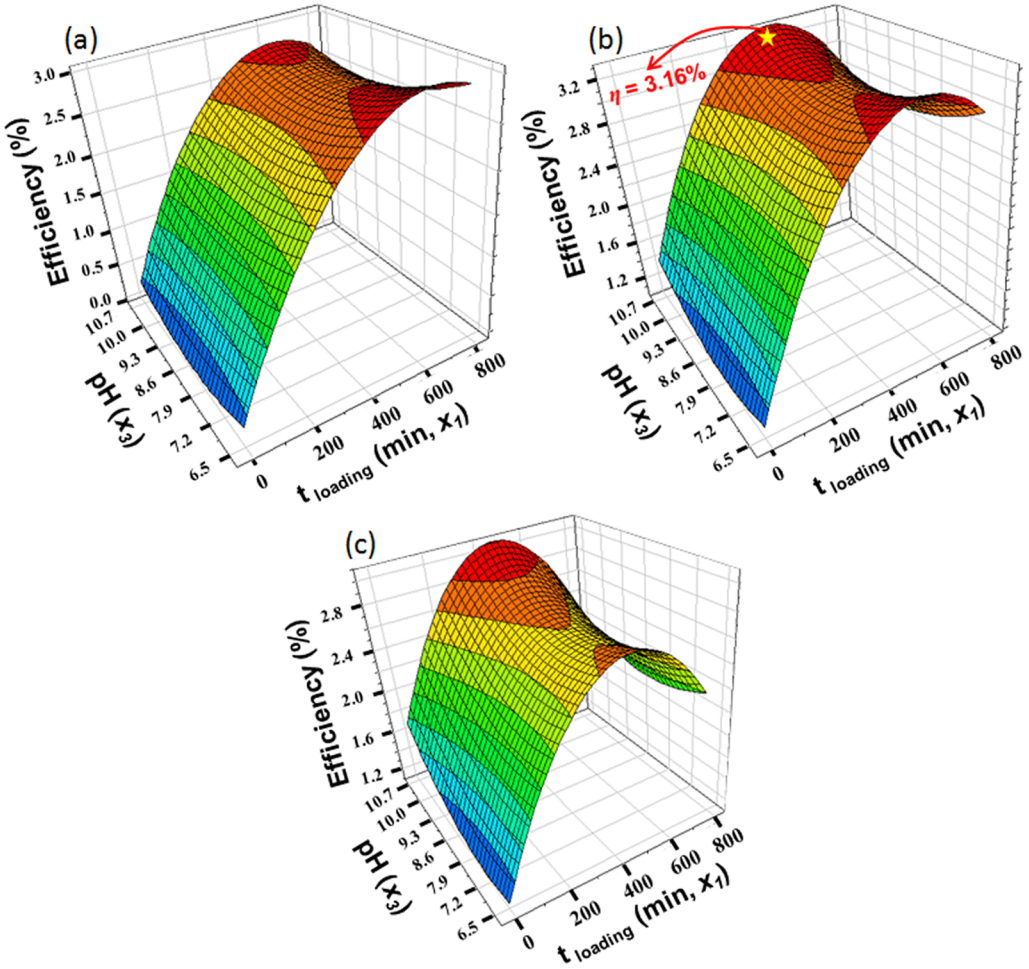

Figure 5. Response surfaces showing the effect of dye loading time (x_1) and pH of dye solution (x_3) on the light-to-electricity conversion efficiency of DSCs assembled with flowerlike microparticle photoanodes, as a function of the dye solution concentration (x_2): (a) 0.05 mM; (b) 0.40 mM; (c) 0.75 mM.

$$y(\%) = 2.86(\pm0.11) + 0.87(\pm0.08)x_1 + 0.18(\pm0.08)x_2 + 0.07(\pm0.08)x_3 - 0.99(\pm0.16){x_1}^2 - 0.44(\pm0.16){x_2}^2 + 0.25(\pm0.16){x_3}^2 - 0.42(\pm0.09)x_1x_2 - 0.08(\pm0.09)x_1x_3 + 0.02(\pm0.09)x_2x_3 \quad (1)$$

where y (%) is the light-to-electricity conversion efficiency, x_1 is the dye loading time, x_2 is the dye solution concentration, and x_3 is the pH of dye solution. The coefficients indicate the importance of each factor in the equation.

It is interesting to note that the coefficients of x_1 and x_2 are positive, while those of the quadratic effects are negative: this means that a slight increase in x_1 and x_2 leads to an increase of DSC performance, but higher values of these factors lead to a reduction in device efficiency. It can be assumed that beyond a certain value of dye impregnation time and dye concentration, protons derived from the Ru-complexes make the dye-loading solution relatively acidic and dissolve ZnO, generating Zn^{2+}/dye aggregates.[39] Such aggregates are harmful to the cell because they lower the electron injection efficiencies and fill the nanosized pores of the ZnO photoanode. On the other hand, the coefficient of x_3 is not very significant, while its quadratic term is positive, indicating that dye solutions with high pH values improve the photovoltaic performance. One possible reason why protons from the carboxyl groups of the dye initiate a dissolution process of the ZnO and form Zn^{2+}/dye complexes is related to the surface properties of the oxide. In particular, the protons adsorbed on the oxide surface dissolve the ZnO, since the pH of the dye solution is much lower than the point of zero charge (pzc) of the metal oxide, defined as the pH where the concentrations of protonated and deprotonated surface groups are equal.[40] The addition of a base to the dye-loading solution, proposed by Keis et al.,[28] makes the pH of the dye solution similar to the pzc of the ZnO, thus reducing the aggregation phenomenon and improving the photovoltaic performance of the cell. Lastly, as regards the interaction terms, only the coefficient of x_1x_2 is significantly negative, indicating that soaking the flowerlike microparticles with a concentrated solution of dye for a long time is counter-productive. Thus, the residence time of ZnO photoanode in the dye has to be shortened when using concentrated dye solution, in view of limiting the dissolution of ZnO during the dye loading.

The fitted response surfaces of the CCF-DoE are reported in Figure 5, where the maximum response zone for sunlight conversion efficiency is observed at x_1 = 391 min, x_2 = 0.40 mM, and x_3 = 10.7. In order to validate the experimental model, two hypotheses were analyzed: (i) H_0: dependency between

the variables does not exist. (ii) H_1: dependency between the variables exists. Student's t test was applied using the quadratic differences between the results and their average, giving a probability of 5% for H_0 and a probability of 95% for H_1, thus corroborating H_1: dependency between the variables exists.

Finally, in order to further support the statistical model, a cross-validation process was carried out: it is a model validation technique for assessing how the fitted results of a chemometric model will generalize to an independent data set. On a practical level, the software proposed some new experiments to be carried out, and also predicted the result to be experimentally obtained. The validation of the chemometric model is achieved if the obtained experimental results are, with 95% confidence, adherent to the predicted ones. This was actually the case, meaning that the chemometric model presented here is robust and valid.

3.3. Investigation on *N*-Methylbenzimidazole as Liquid Electrolyte Additive for ZnO-Based DSCs. Once the best conditions for the preparation procedure of the flowerlike microparticle-based photoanodes are identified, a further increase in photovoltaic performance can be accomplished by including additives to the commercial liquid electrolyte. While for TiO_2-based cells a large number of investigations on liquid electrolyte additives were reported in several reviews,[41,42] the effect of additives for ZnO-based cells has not been adequately addressed yet. In particular, the effect of *N*-methylbenzimidazole (NMBI), usually added to standard liquid electrolytes for TiO_2-based DSCs, but never tested in the presence of ZnO photoelectrodes, was investigated. Concerning TiO_2-based devices, NMBI was generally reported to increase the V_{oc} of DSC, since it adsorbs onto the surface of TiO_2.[41,42] In addition, Yang et al.[43] found that this additive had a positive effect on ionic conductivity and apparent diffusion coefficient of triiodide, $D_{app}(I_3^-)$, weakening the Coulomb force between the cation and the anion, thus facilitating ion dissociation.

In this work, the effect of NMBI was investigated for DSCs assembled with the photoanode prepared according to the optimal conditions (experiment F12 in Table 1), and the results are reported in Table 2 and in Figure 6.

Table 2. Photovoltaic Performances of DSCs Assembled with the Optimized ZnO Flowerlike Microparticle-Based Photoanode and with the Addition of NMBI as a Liquid Electrolyte Additive at Different Concentrations

electrolyte	J_{sc} (mA/cm^2)	V_{oc} (V)	FF	η (%)
AN 50	8.57	0.56	0.65	3.16
AN 50 + NMBI 0.25 M	8.75	0.58	0.65	3.26
AN 50 + NMBI 0.5 M	9.47	0.59	0.64	3.59
AN 50 + NMBI 0.75 M	9.18	0.59	0.62	3.35

As it can be noted, the addition of NMBI leads to an increase of both J_{sc} and V_{oc}. This result seems to confirm that the two effects observed by Yang et al.[43] for the TiO_2-based photoanode occur even in the presence of a ZnO-based one. In particular, in the presence of 0.5 M NMBI, the highest efficiency of the devices assembled with ZnO flowerlike microparticle-based photoanodes was obtained: 3.59% (J_{sc} = 9.47 mA/cm^2, V_{oc} = 0.59 V, FF = 0.64). From the data reported in Table 2, it seems that the NMBI effect in reducing the electron recombination was maximized by using the concentration of 0.5 M.

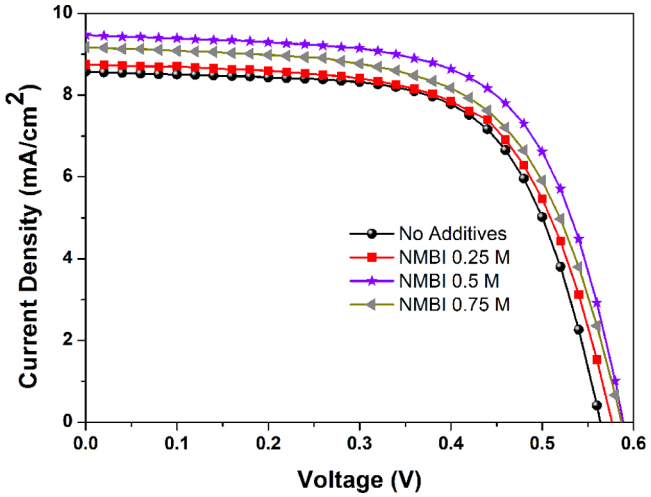

Figure 6. Current density−voltage curves of DSCs assembled with the best ZnO flowerlike microparticle-based photoanode (experiment F12 in Table 1) and with the addition of NMBI as a liquid electrolyte additive at different concentrations.

In order to further confirm the above-mentioned hypothesis, electrochemical impedance spectroscopy measurements on the NMBI-based cells were performed and the results were compared with the reference cell (i.e., experiment F12 in Table 1). In Figure 7, examples of Nyquist plots of cell

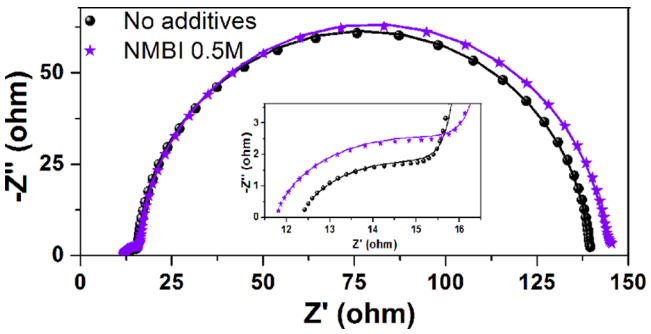

Figure 7. Nyquist plots of DSCs assembled with the best ZnO flowerlike microparticle-based photoanode (experiment F12 in Table 1) and with the addition of NMBI as a liquid electrolyte additive acquired at the open circuit voltage. The points are experimental data while the continuous lines are fitting curves.

impedances are reported. In a typical impedance spectrum of a DSC, three arcs can be distinguished: a main arc related to the recombination at the oxide/electrolyte interface, and two side arcs related to the charge transfer at the electrolyte/counter electrode interface and to the diffusion of charges in the electrolytic solution. Moreover, a small feature related to the charge transport inside the oxide material should be visible in the high frequency region, quite overlapping with the counter electrode impedance.[44] In Figure 7, the arcs related to the diffusion cannot be observed due to the lowest frequency value measured (usually the characteristic time constant of this process lies in the range 1−100 s).[45] In contrast, the high frequency arcs related to the counter electrode are quite superimposed for the two kinds of devices, meaning that the presence of the additive has no influence on the charge transfer between the Pt and the solution. On the other hand, it can be noted that the main arc exhibited by the NMBI-based cell is

taller and wider than the one obtained from the device fabricated without additives: in accordance with the results of Yang et al. (despite using a different semiconductor),[43] the presence of NMBI is effective in increasing the charge lifetime, witnessed by a larger recombination resistance (basically equal to arc radius).

To quantitatively evaluate the charge recombination and the transport properties in the flowerlike based photoanode, the experimental impedance spectra were fitted through an equivalent circuit.[44] The results of the fitting procedure are shown in Figure 7 superimposed to the experimental curves, evidencing a good match between the measured and calculated spectra. The electron lifetime τ_n and the diffusion coefficient D_n were evaluated from the fitting parameters,[45] and in Figure 8

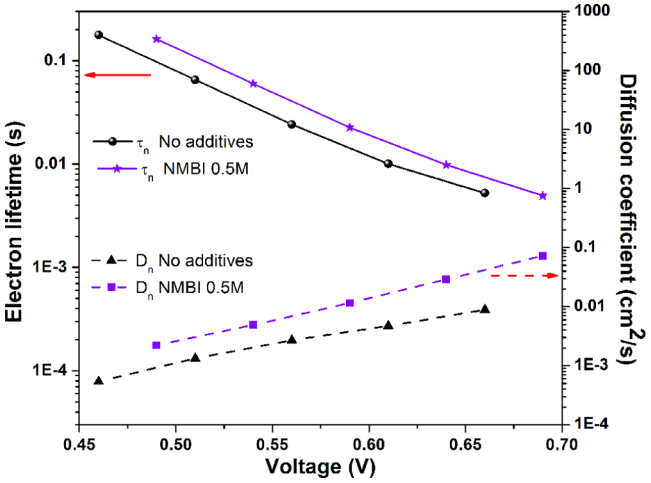

Figure 8. Electron lifetime and diffusion coefficient dependence on the applied voltage for DSCs assembled with the optimized ZnO flowerlike microparticle-based photoanode and with the addition of NMBI as liquid electrolyte additive.

they are reported as a function of the applied bias voltage. In agreement with what was observed from the Nyquist plots, the lifetime values of NMBI-based cells are larger with respect to those of the reference cell; the reduction of the charge recombination is therefore the reason for the higher photovoltage exhibited by the NMBI-containing devices.[46] In addition, the electron diffusion coefficient of these cells is higher than the reference one. Differently from what was reported by Yang et al.,[43] the triiodide apparent diffusion coefficient was not assessable due to frequency limitation. However, it was found that the inclusion of NMBI has a positive effect also on the oxide transport properties, thus further increasing the collection efficiency and, as a consequence, the short circuit current density.[25] Overall, it was shown that the addition of NMBI is a valuable means of increasing the performance of DSCs assembled with ZnO photoelectrodes.

CONCLUSIONS

Promising photovoltaic properties of ZnO flowerlike microstructures were demonstrated. ZnO microparticles were synthesized by a simple, reproducible and low-cost hydrothermal process, thus obtaining wurtzite-like crystalline structures as evidenced by detailed morphological characterization. After dispersion of ZnO flowerlike particles in the acetic acid-based solution, a 14 μm-thick ZnO layer acting as DSC photoanode was fabricated. ZnO-based DSCs were assembled with a customized microfluidic architecture proposed by our group and their photovoltaic properties were evaluated. A chemometric approach was used, for the first time with ZnO-based DSCs, with the purpose of establishing the best sensitization conditions, thus avoiding Zn^{2+}/dye complex formation. A maximum photoconversion efficiency value of 3.16% was achieved. The efficiency was enhanced up to 3.59% when adding, as unprecedently reported in the presence of a ZnO photoanode, *N*-methylbenzimidazole into the liquid electrolyte. This effect was attributed to the reduction of charge recombination and to the enhancement of the diffusion coefficient, as evidenced by EIS analysis.

ASSOCIATED CONTENT

Supporting Information

Factorial hypercube of a central composite face-centered (CCF) DoE, nitrogen sorption measurement, DFT pore size distribution, and chemometric model fitting data. This material is available free of charge via the Internet at http://pubs.acs.org.

AUTHOR INFORMATION

Corresponding Author

*Phone: +39 011 090 7381. Fax: +39 011 090 7399. E-mail: diego.pugliese@polito.it.

Notes

The authors declare no competing financial interest.

ACKNOWLEDGMENTS

The authors would like to acknowledge Dr. Angelica Chiodoni and Dr. Edvige Celasco for FESEM characterizations.

ABBREVIATIONS

ZnO, zinc oxide; TiO_2, titanium dioxide; DSC, dye-sensitized solar cell; FTO, fluorine-doped tin oxide; SnO_2, tin oxide; In_2O_3, indium oxide; 1-D, monodimensional; *I*–*V*, current–voltage; IPCE, incident photon-to-electron conversion efficiency; EIS, electrochemical impedance spectroscopy; KOH, potassium hydroxide; $ZnNO_3{\cdot}6H_2O$, zinc nitrate hexahydrate; FESEM, field emission scanning electron microscopy; BET, Brunauer–Emmett–Teller; DFT, density functional theory; XRD, X-ray diffraction; AM, air mass; G, global; QTH, quartz tungsten halogen; AC, alternating current; DoE, design of experiments; CCF, central composite face-centered; JCPDS, Joint Committee on Powder Diffraction Standards; FF, fill factor; pzc, point of zero charge; NMBI, *N*-methylbenzimidazole

REFERENCES

(1) O'Regan, B.; Grätzel, M. *Nature* **1991**, *353*, 737–740.
(2) Grätzel, M. *Prog. Photovoltaics Res. Appl.* **2006**, *14*, 429–442.
(3) Bella, F.; Bongiovanni, R. *J. Photochem. Photobiol., C* **2013**, *16*, 1–21.
(4) Nazeeruddin, M. K.; Klein, C.; Liska, P.; Grätzel, M. *Coord. Chem. Rev.* **2005**, *249*, 1460–1467.
(5) Yella, A.; Lee, H. W.; Tsao, H. N.; Yi, C.; Chandiran, A. K.; Nazeeruddin, M. K.; Diau, E. W. G.; Yeh, C. Y.; Zakeeruddin, S. M.; Grätzel, M. *Science* **2011**, *334*, 629–634.
(6) (a) Yoshida, T.; Terada, K.; Schlettwein, D.; Oekermann, T.; Sugiura, T.; Minoura, H. *Adv. Mater.* **2000**, *12*, 1214–1217. (b) Kay, A.; Grätzel, M. *Chem. Mater.* **2002**, *14*, 2930–2935. (c) Jana, A. K. *J. Photochem. Photobiol., A* **2000**, *132*, 1–17. (d) Sayama, K.; Sugihara, H.; Arakawa, H. *Chem. Mater.* **1998**, *10*, 3825–3832.

(7) Look, D. C. *Mater. Sci. Eng., B* **2001**, *80*, 383−387.
(8) Cao, H.; Xu, J. Y.; Zhang, D. Z.; Chang, S. H.; Ho, S. T.; Seelig, E. W; Liu, X.; Chang, R. P. H. *Phys. Rev. Lett.* **2000**, *84*, 5584−5587.
(9) Gayen, R. N.; Dalui, S.; Rajaram, A.; Pal, A. K. *Appl. Surf. Sci.* **2009**, *255*, 4902−4906.
(10) Gomez, J. L.; Tigli, O. *J. Mater. Sci.* **2013**, *48*, 612−624.
(11) Podrezova, L. V.; Porro, S.; Cauda, V.; Fontana, M.; Cicero, G. *Appl. Phys. A: Mater. Sci. Process.* **2013**, DOI: 10.1007/s00339-013-7838-5.
(12) Zhang, Q.; Dandeneau, C. S; Zhou, X.; Cao, G. *Adv. Mater.* **2009**, *21*, 1−22.
(13) Martinson, A. B. F.; Elam, J. W; Hupp, J. T; Pellin, M. J. *Nano Lett.* **2007**, *7*, 2183−2187.
(14) Wang, X. D.; Ding, Y.; Summers, C. J.; Wang, Z. L. *J. Phys. Chem. B* **2004**, *108*, 8773−8777.
(15) Xiang, J. H.; Zhu, P. X.; Masuda, Y.; Okuya, M.; Kaneko, S.; Koumoto, K. *J. Nanosci. Nanotechnol.* **2006**, *6*, 1797−1801.
(16) Tiwari, A.; Snure, M. *J. Nanosci. Nanotechnol.* **2008**, *8*, 3981−3987.
(17) Calestani, D.; Zha, M.; Mosca, R.; Zappettini, A.; Carotta, M. C.; Di Natale, V.; Zanotti, L. *Sens. Actuators, B* **2010**, *144*, 472−478.
(18) Arnold, M. S.; Avouris, P.; Pan, Z. W.; Wang, Z. L. *J. Phys. Chem. B* **2003**, *107*, 659−663.
(19) Johnson, J.; Yan, H.; Yang, P.; Saykally, R. *J. Phys. Chem. B* **2003**, *107*, 8816−8828.
(20) Bai, X. D.; Wang, E. G.; Gao, P. X.; Wang, Z. L. *Nano Lett.* **2003**, *3*, 1147−1150.
(21) Kong, X. Y.; Wang, Z. L. *Nano Lett.* **2003**, *3*, 1625−1631.
(22) Farías Rivera, V.; Auras, F.; Motto, P.; Stassi, S.; Canavese, G.; Celasco, E.; Bein, T.; Onida, B.; Cauda, V. *Chem.—Eur. J.* **2013**, *19*, 14665−14674.
(23) Ranga Rao, A.; Dutta, V. *Nanotechnology* **2008**, *19*, 445712−445720.
(24) Bauer, C.; Boschloo, G.; Mukhtar, E.; Hagfeldt, A. *J. Phys. Chem. B* **2001**, *105*, 5585−5588.
(25) Hagfeldt, A.; Boschloo, G.; Sun, L.; Kloo, L.; Pettersson, H. *Chem. Rev.* **2010**, *110*, 6595−6663.
(26) Memarian, N.; Concina, I.; Braga, A.; Rozati, S. M.; Vomiero, A.; Sberveglieri, G. *Angew. Chem., Int. Ed.* **2011**, *50*, 1−6.
(27) Chou, T. P.; Zhang, Q.; Cao, G. *J. Phys. Chem. C* **2007**, *111*, 18804−18811.
(28) Keis, K.; Magnusson, E.; Lindstrom, H.; Lindquist, S. E.; Hagfeldt, A. *Sol. Energy Mater. Sol. Cells* **2002**, *73*, 51−58.
(29) Saito, M.; Fujihara, S. *Energy Environ. Sci.* **2008**, *1*, 280−283.
(30) Kakiuchi, K.; Hosono, E.; Fujihara, S. *J. Photochem. Photobiol., A* **2006**, *179*, 81−86.
(31) Lamberti, A.; Gazia, R.; Sacco, A.; Bianco, S.; Quaglio, M.; Chiodoni, A.; Tresso, E.; Pirri, C. F. *Prog. Photovoltaics Res. Appl.* **2012**, DOI: 10.1002/pip.2251.
(32) Bella, F.; Pugliese, D.; Nair, J. R.; Sacco, A.; Bianco, S.; Gerbaldi, C.; Barolo, C.; Bongiovanni, R. *Phys. Chem. Chem. Phys.* **2013**, *15*, 3706−3711.
(33) Chen, P.; Gu, Li.; Xue, X.; Song, Y.; Zhu, L.; Cao, X. *Mater. Chem. Phys.* **2010**, *122*, 41−48.
(34) Pugliese, D.; Shahzad, N.; Sacco, A.; Musso, G.; Lamberti, A.; Caputo, G.; Tresso, E.; Bianco, S.; Pirri, C. F. Fast TiO_2 sensitization using the semisquaric acid as anchoring group. *Int. J. Photoenergy*, accepted.
(35) Beebe, K. R.; Pell, R. J.; Seasholtz, M. B. In *Chemometrics: a practical guide*; John Wiley & Sons, Inc.: 1998.
(36) Fricke, J.; Pohlmann, K.; Jonescheit, N. A.; Ellert, A.; Joksch, B.; Luttmann, R. *Biotechnol. J.* **2013**, *8*, 738−747.
(37) Bella, F.; Nair, J. R.; Gerbaldi, C. *RSC Adv.* **2013**, *3*, 15993−16001.
(38) Lundstedt, T.; Seifert, E.; Abramo, L.; Thelin, B.; Nyström, A.; Pettersen, J.; Bergman, R. *Chemom. Intell. Lab. Syst.* **1998**, *42*, 3−40.
(39) Keis, K.; Lindgren, J.; Lindquist, S. E.; Hagfeldt, A. *Langmuir* **2000**, *16*, 4688−4694.
(40) Keis, K.; Bauer, C.; Boschloo, G.; Hagfeldt, A.; Westermark, K.; Rensmo, H.; Siegbahn, H. *J. Photochem. Photobiol., A* **2002**, *148*, 57−64.
(41) Yu, Z.; Vlachopoulos, N.; Gorlov, M.; Kloo, L. *Dalton Trans.* **2011**, *40*, 10289−10303.
(42) Wang, M.; Grätzel, C.; Zakeeruddin, S. M.; Grätzel, M. *Energy Environ. Sci.* **2012**, *5*, 9394−9405.
(43) Yang, H.; Liu, J.; Lin, Y.; Zhang, J.; Zhou, X. *Electrochim. Acta* **2011**, *56*, 6271−6276.
(44) Sacco, A.; Lamberti, A.; Gazia, R.; Bianco, S.; Manfredi, D.; Shahzad, N.; Cappelluti, F.; Ma, S.; Tresso, E. *Phys. Chem. Chem. Phys.* **2012**, *14*, 16203−16208.
(45) Bella, F.; Ozzello, E. D.; Sacco, A.; Bianco, S.; Bongiovanni, R. *Int. J. Hydrogen Energy* **2013**, DOI: 10.1016/j.ijhydene.2013.06.110.
(46) Cicero, G.; Musso, G.; Lamberti, A.; Camino, B.; Bianco, S.; Pugliese, D.; Risplendi, F.; Sacco, A.; Shahzad, N.; Ferrari, A. M.; Ballarin, B.; Barolo, C.; Tresso, E.; Caputo, G. *Phys. Chem. Chem. Phys.* **2013**, *15*, 7198−7203.